THERMO-STRUCTURAL ANALYSIS OF THE SEPARATION SYSTEM OF VLS PAYLOAD

Humberto Araujo Machado, humbertoam@iae.cta.br
Cláudio Gilberto Bautzer dos Santos, bautzer@iae.cta.br
Instituto de Aeronáutica e Espaço- IAE, Pç. Mal. Eduardo Gomes, 50, Vila das Acácias, São José dos Campos, SP, 12228-904

Abstract. *In this work the effect of the aerodynamic heating over the structural behavior of the payload separation system of VLS (Satellite Launcher Vehicle), that has being developed by IAE (Institute of Aeronautics and Space), is analyzed. First, the thermal problem is solved, and the temperature distribution is obtained in the region of the separation belt. After, the resulting temperature field is employed to estimate the mechanical properties and the thermal tensions generated by the temperature gradients. The calculation is performed through the commercial software ABAQUS. Results allow evaluating if the separation system complies the strength requirements during the most critical phases of flight.*

Keywords: Numerical simulation; Separation system; Thermal analysis

1. INTRODUCTION

Space and sub orbital vehicles reach high speeds within the atmosphere, i.e., below 100 km of altitude. Such high velocities result in aerodynamic heating. In the case of recoverable payloads, the heating occurs in both, ascendant and re-entry trajectories. Air temperature surpasses 2000° C at the stagnation point (Machado & Pessoa Filho, 2007). As a consequence, aerodynamic heating plays a very important role in the vehicle design. The effects of high temperatures on the mechanical behavior of the structure have to be carefully investigated.

In this work the thermal stresses are evaluated in the belt of the payload separation system of VLS (*Satellite Launcher Vehicle*), Fig. 1, that have being under development by IAE (*Institute of Aeronautics and Space*), considering the effect of the temperature over the mechanical properties of the diverse materials. The results are analyzed taking into account the capacity to attend the solicitations.
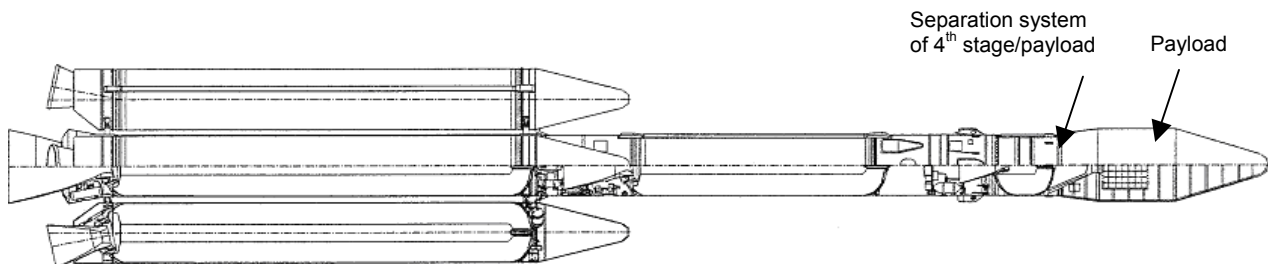
Figure 1. VLS (*Satellite Vehicle Launcher*) and region of study.

2. PHYSICAL PROBLEM

VLS is a four-stage solid propellant rocket. Its trajectory is showed in Fig. 2. The geometry of separation system of 4th stage/payload is showed in Fig. 3. The belt is placed externally between the stage and the payload.
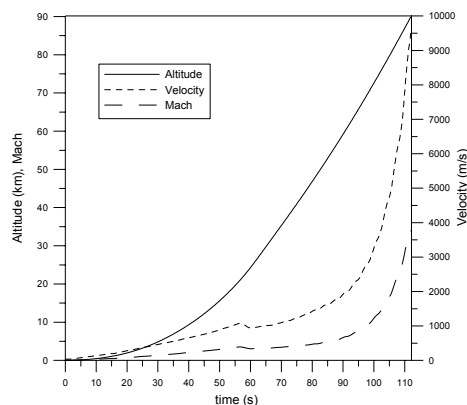
Figure 2. VLS trajectory (Gauthier, 1989)
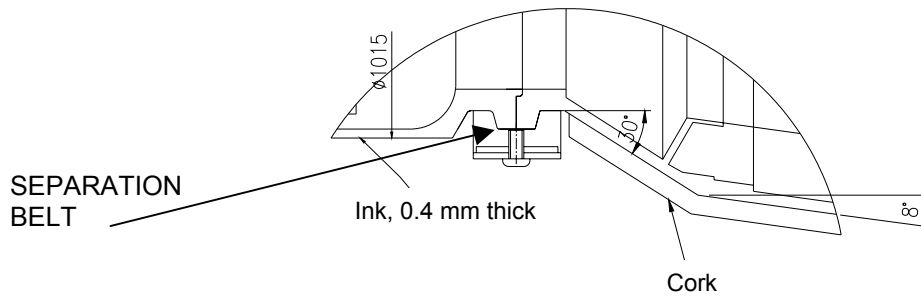
Figure 3. Geometry of separation system of 4th stage/payload.

2.1. Heat exchange

To predict the heat transfer on VLS surface, it is necessary to know pressure, temperature and velocity fields around the vehicle. That can be accomplished by numerically solving the boundary layer equations. However, such a procedure is expensive and time consuming. In the present work a simpler, but reliable, engineering approach is used. The following simplifying assumptions are made:
- Zero angle of attack;
- VLS rotation around its longitudinal axis is neglected;
- Atmospheric air is considered to behave as a calorically and thermally perfect gas (no chemical reactions); and

The free stream conditions ahead of the nose cap are those given by v_∞, T_∞, p_∞, corresponding, respectively, to velocity, temperature and pressure. By knowing v_∞ and altitude, as function of time, together with an atmospheric model (U.S. Standard Atmosphere, 1976), it is possible to evaluate the free stream properties, such as p_∞, T_∞, and c_∞, which represent free stream pressure, temperature and speed of sound, respectively. For supersonic flow ($M_\infty > 1$), a detached shock wave appears ahead of the nose. By using the normal shock relationships (Anderson, 1990), it is possible to calculate v_1, T_1 and p_1 after the shock.

The heat flux over the external surface was calculated through the Zoby's method (Zoby et al, 1981; Miranda & Mayall, 2001), namely:

$$q = H\,(T_{aw} - T_w) \tag{1}$$

where q is heat flux, T_w is the wall temperature and T_{aw} is the adiabatic wall temperature, also called recovery temperature, T_r, given by:

$$T_{aw} = T_e + F_R \frac{v_e^2}{2c_p} \tag{2}$$

where c_p is the specific heat, T_e the temperature and v_e the velocity. The subscript e refers to conditions at the boundary layer edge. F_R is the recovery factor, equal to $\sqrt{Pr_w}$, for laminar flow and $\sqrt[3]{Pr_w}$ for turbulent flow. Pr_w is the Prandtl number evaluated at wall temperature, $Pr_w = 0.71$. The convective heat transfer coefficient comes from the Reynolds analogy, namely:

$$H = 0.5 \rho_e c_p v_e \, Pr_w^{-a} \, C_F \tag{3}$$

where a is equal to 0.6 for laminar flow and 0.4 for turbulent flow. To take into account compressibility effects, a modified friction factor is obtained (Anderson, 1989)

$$C_F = K_1 \left(Re_\theta\right)^{K_2} \left(\frac{\rho_e^*}{\rho_e}\right)\left(\frac{\mu_e^*}{\mu_e}\right)^{K_3} \tag{4}$$

In the equation above, Re_θ is the Reynolds number, based on the boundary layer thickness, θ:

$$Re_\theta = \frac{\rho_e V_e \theta}{\mu_e} \tag{5}$$

The superscript "*" refers to properties evaluated at Eckert's reference temperature (T_e*). Viscosity, μ, is evaluated according to Sutherland´s equation, as function of temperature (Anderson, 1989) and ρ is the specific mass. In Eq.(4) $K_1 = 0.44$, $K_2 = -1$ and $K_3 = 1$, for laminar flow. For turbulent flow, $K_2 = K_3 = -m$, and

$$K_1 = 2\left(\frac{1}{C_5}\right)^{\frac{2N}{N+1}}\left[\frac{N}{(N+1)(N+2)}\right]^m$$ (6.a)

$$m = \frac{2}{N+1}$$ (6.b)

$$C_5 = 2.2433 + 0.93N$$ (6.c)

$$N = 12.76 - 6.5\log_{10}(Re_\theta) + 1.21[\log_{10}(Re_\theta)]^2$$ (6.a)

For laminar flow, the boundary layer momentum thickness is given by (Anderson, 1989):

$$\theta_L = \frac{0.664\left(\int_0^y \rho_e^* \mu_e^* v_e R^2 dy'\right)^{\frac{1}{2}}}{\rho_e v_e R}$$ (7)

where y is measured along the body's surface and $y=0$ corresponds to the stagnation point, and R is a geometric parameter schematically shown in Fig. 4, were the curved red line represents the nose cap surface.
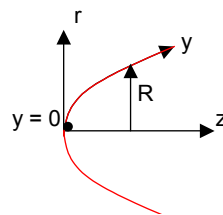
Figure 4. Coordinate system.

In this work the numerical integration of Eq. (7) was obtained according to the trapezoidal method. As $R \to 0$, Eq. (7) becomes undetermined. By taking the limit of Eq. (7) as $R \to 0$, the following expression is obtained (Miranda & Mayall, 2001):

$$\theta_L = \frac{0.332\left(\rho_e^* \mu_e^*\right)^{\frac{1}{2}}}{\rho_e \sqrt{\frac{1}{R_N}\left[\frac{2(p_s - p_\infty)}{\rho_s}\right]^{\frac{1}{2}}}}$$ (8)

In this work Eq. (8) is applied for $y < 0.1 R_N$, where R_N is the radius of curvature at the stagnation point.
The boundary layer thickness for turbulent flow is obtained by solving the following first order differential equation:

$$\frac{D(\rho_e v_e R \theta_T)}{Dy} = 0.5 C_F \rho_e v_e R$$ (9)

After obtaining the boundary layer momentum thickness, θ, Re_θ, C_F and H can be evaluated by using Eqs. (5), (4) and (3), respectively. Along the transition region between laminar and turbulent flow, the following relationship is used[11]:

$$q_{Tr} = q_L + F(y)(q_T - q_L)$$ (10)

where the subscripts Tr, L and T represent, respectively, transitional, laminar and turbulent flow. The transitional factor, $F(y)$, is given by (Dhavan & Narasinha, 1958):

$$F(y) = 1 - exp\left\{-0.412\left[\frac{4.74(y - y_L)}{(y_T - y_L)}\right]\right\} \qquad (11)$$

Transition is supposed to occur for $163 < Re_\theta < 275$.

Properties evaluation at the boundary layer edge is performed assuming isentropic flow between the stagnation region and the location "i" where properties are needed, namely

$$\rho_{e,i} = \rho_s\left(\frac{p_{e,i}}{p_s}\right)^{\frac{1}{\gamma}} \qquad (12.a)$$

$$h_{e,i} = h_s\left(\frac{p_{e,i}}{p_s}\right)^{\frac{\gamma-1}{\gamma}} \qquad (12.b)$$

$$v_{e,i} = \sqrt{2(h_s - h_{e,i})} \qquad (12.c)$$

$$T_{e,i} = \frac{h_{e,i}}{c_p} \qquad (12.d)$$

The local pressure, $p_{e,i}$, is obtained from the modified Newton´s method (Anderson, 1989; Machado & Villas-Boas, 2006) and $\gamma=1.4$. The subscript "s" appearing in Eqs. (12) refers to the stagnation condition. Eckert's reference temperature is obtained from (Anderson, 1989):

$$\frac{T_{e,i}^*}{T_{e,i}} = 1 + 0.032M_{e,i}^2 + 0.58\left(\frac{T_W}{T_{e,i}} - 1\right) \qquad (13)$$

The solution procedure can be summarized as follows:
   i.   From a given trajectory the US Standard Atmosphere (1976) is used to obtain the free stream properties, including the stagnation ones;
   ii.   Normal shock relationships are used to obtain the fluid flow properties behind the shock;
   iii. By using the modified Newton method, pressure distribution is obtained along the payload;
   iv.   Equations (12) provide the local properties at the boundary layer edge;
   v.   If $y < 0.1 R_N$, Eq. (8) provides the laminar boundary layer thickness, leading to the estimation of Re_θ, C_F and H, provided by Eqs. (5), (4) and (3), respectively;
   vi.   If $y > 0.1 R_N$ and $Re_\theta < 163$, Eq. (7) is numerically integrated up to the location where the momentum thickness is to be estimated. Such an integration is performed by using the trapezoidal method;
   vii. If $y > 0.1 R_N$ and $Re_\theta > 275$, Eq. (9) is numerically integrated by the trapezoidal rule leading to the turbulent boundary layer thickness;
   viii. If $y > 0.1 R_N$ and $163 < Re_\theta < 275$, Eqs. (10) and (11) are used to estimate H;
It should be pointed out that such a procedure is performed along the payload's surface (following the y-coordinate), for different trajectory times. Therefore, $H=H(y,t)$.

The Zoby's Method is applicable to smooth surfaces with some precision. However, the region of the separation system cannot be considered a smooth region, due the presence of cavities and protuberances were recirculations are formed and make it hard to determine h (Surber, 1965). In order to determine the values of the convection coefficient in the belt, the correlation presented by Cline (1969) is used to obtain average values of h as function of local Reynolds and Mach Numbers:

$$\frac{h}{h_0} = \frac{22M_e}{Re_e^{0.15}} \qquad (14)$$

where:
h – convection coefficient in the irregular region (protuberance/cavity)
h_o – – convection coefficient at the VLS stagnation point
M_e – local mach number in the boundary layer edge.
Re_e – Local Reynolds Number (based on the extension of y-coordinate)

This correlation presents limitations to be applied. The data used for your construction were obtained until the limit of Mach 4.44 (that is reached at 82.5 s of flight), with a dispersion of about 20 %. The value obtained corresponds to the maximum value reached by *h* in the vicinity of the protuberance/cavity and occurs in specific points. The average should tend to values quite lower.

2.3. Thermal boundary conditions

The boundary conditions used for the energy equations are adiabatic wall for the internal surface and for the external surface where it is covered by cork. The convective heat transfer coefficient and external air temperature during the trajectory were used to estimate the wall temperature during the flight. The resulting wall temperature at the belt external surface was interpolated by a polynomial (named *curve T*), and applied over the exposed surfaces of the separation belt, Fig. 5. Initial conditions are 27° C for the whole domain.
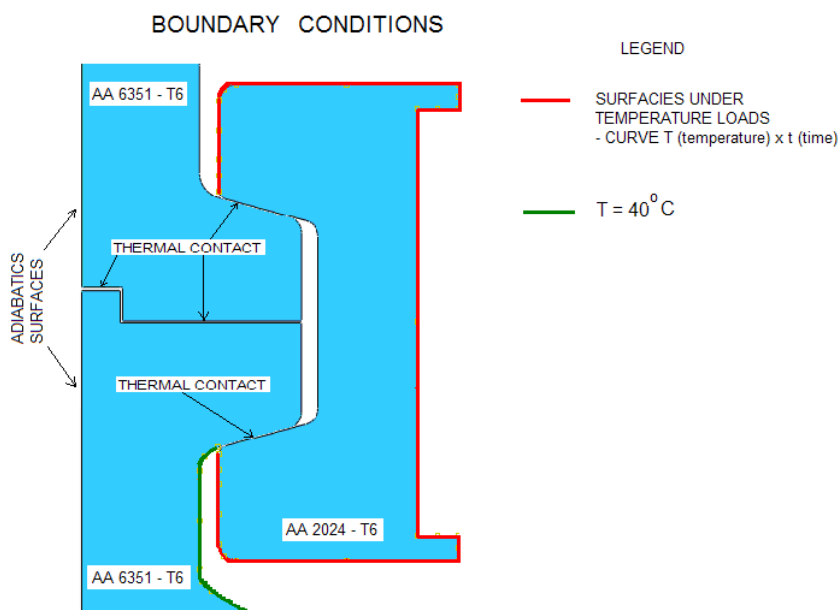
Figure 5. Temperature boundary conditions applied to the simulation domain.

3. METHODOLOGY

The thermo-elastic analysis was realized with ABAQUS software package (Dassault Systèmes, 2007) based in the Finite Element Method (FEM). The structural analysis is composed for two steps: a thermal analysis, where the temperature distribution within the structure is determined, followed by a mechanical analysis considering such distribution previously calculated. The contact between the surfaces was simulated in both analyses with thermal and mechanical contact elements, respectively, and the structural system was discretized with axissimetric elements. In this analysis all aerodynamic loads and specific loads of the separation system were neglected, since the main objective of this work is to analyze the structural behavior under the thermal loads. Typical mechanical properties used in the structure are showed in Tab.1. The properties of the material were considered as functions of the temperature, and its dependence is showed in Fig. 6. Figure 7 shows the whole domain of simulation with the complete structural model and detailed meshing of the region containing the contact surfaces.

Table 1. Material properties (Klausner and Machado, 1998).

Material	Modulus of Elasticity (GPa)	Poissons Ratio	Specific Heat (J/g-°C)	Yield Tensile Strengh (MPa)	Ultimate Tensile Strengh (MPa)
AA 2024 – T6	72.4	0,33	0.875	345	427
AA 6351 – T6	68.9	0.33	0.890	302	323

a) AA 2024

b) AA6351
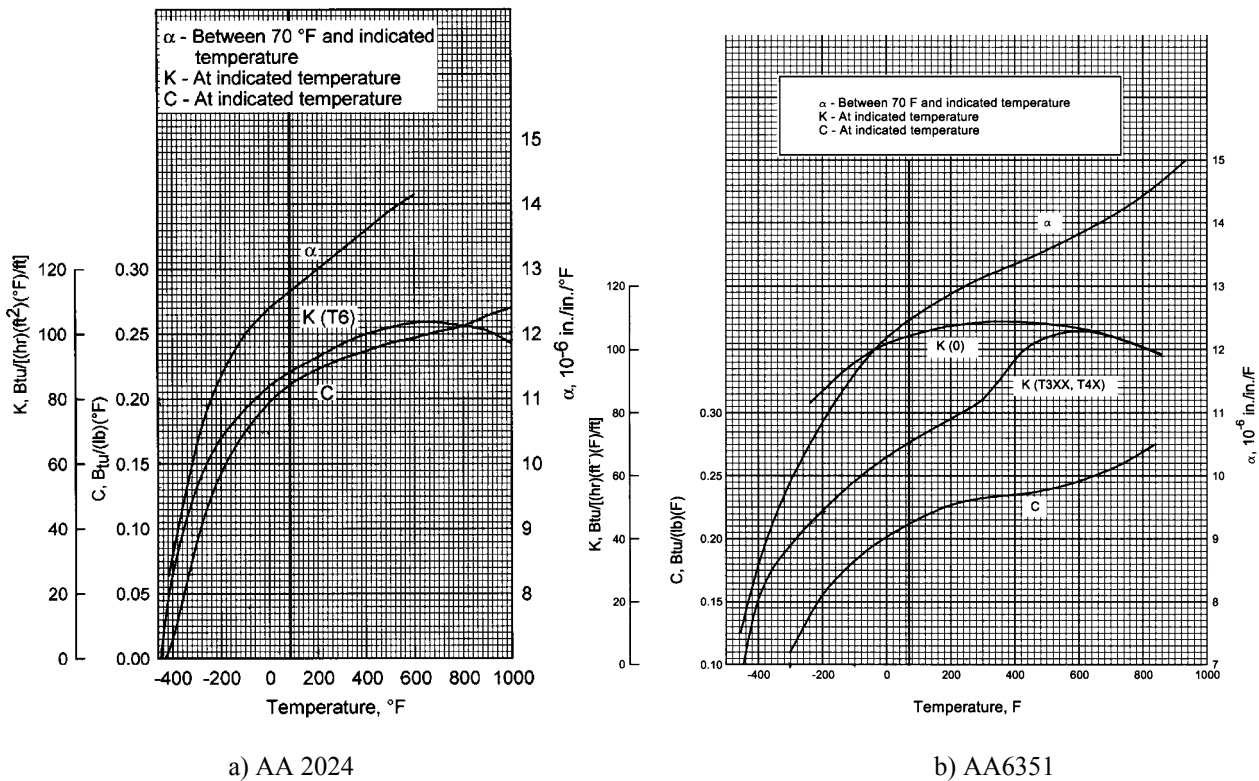
Figure 6. Temperature dependence of the properties of the structure material.
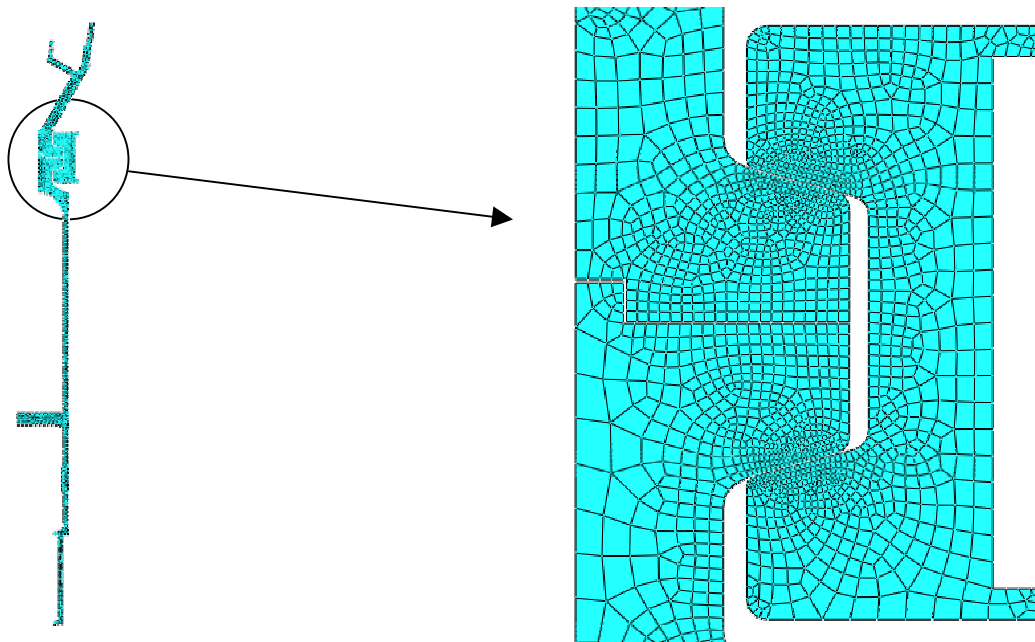
Figure 7. Structural model and contact region.

4. RESULTS

Figure 8 presents the variation of recovery temperature x time over the belt surface. It is remarkable that this temperature rises dramatically during the last 10 seconds of the considered trajectory. However, the convection coefficient reaches its maximum value between 50-60 seconds, and decreases. Since the wall heat flux depends on the product between then (recovery temperature and convection coefficient), the combination produces the highest heat fluxes by the end of the period of flight in atmosphere. In Figures 9.a,b, convective coefficient and external surface temperature of the belt are plotted with the time, considering both, the treatment for a smooth surface and the use of

Eq.(14). As it was expected, *h* and the surface temperature are higher with the use of the correlation. In Figure 9.a, the coefficient *h* tends to zero after 90 seconds. This is a consequence of the atmosphere rarefaction. At this instant, although the vehicle moves about Mach 6, the altitude is above 60 km. In such condition, the correlation presented in Eq. (22) is not trustable, since it still presents high values of *h* when compared to the results for a smooth surface, and would tend to zero.
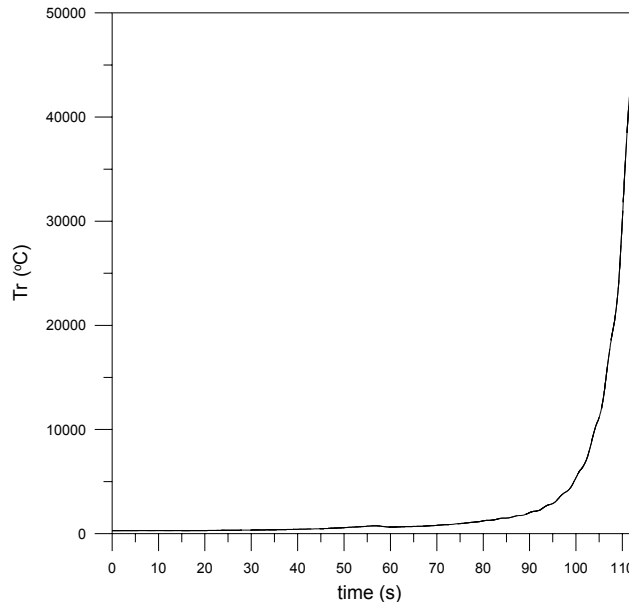
Figure 8. Recovery temperature.
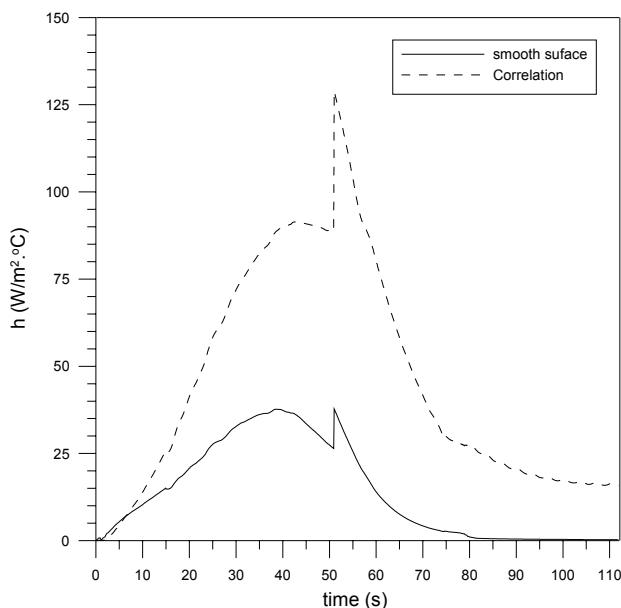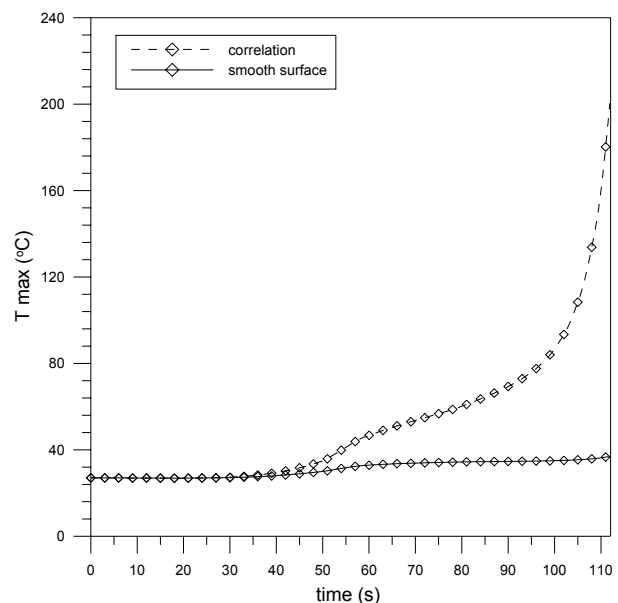
(a) Convection coefficient	(b) Wall maximum temperature

Figure 9. Results for aerodynamic heating

From the results presented for wall temperature, the temperature distribution in the separation system region was calculated, Fig. 10. Due to the contact resistance, temperatures in the belt itself are higher than temperature reached in the structure. Employing that distribution, the Von Mises stresses were calculated, Fig. 11. The maximum value for Von Mises stresses is 277.4 MPa, in the in the internal curvature of the separation belt, Fig. 11. Considering a safety margin of 10 % used in this project for yield stresses and 35 % for ultimate stresses, the resulting margins for each structural material are:
- Yield stresses: AA 2024 + 0.16%, AA6351, -0.011%.
- Ultimate stresses: AA 2024 + 0.14% , AA6351, -0.14%

Although the safety margins for AA 6351 aluminum alloy calculated are low, they are quite close to the ideal margins and this material can be employed in the separation system. One should note that the extreme values for stresses in the belt (414.80 Mpa) is almost punctual, localized in the internal curvatures of the blank region between the belt and the structure. In the most of the region of study, stresses can be considered low when compared to prescribed limits.
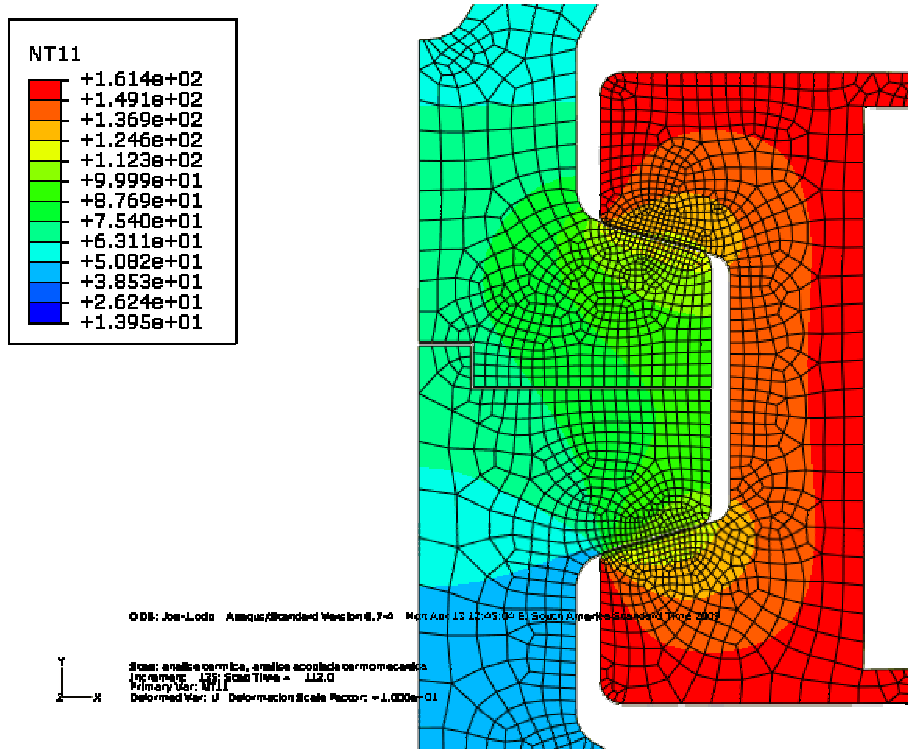
Figure 10. Temperature distribution in the region of the separation system.
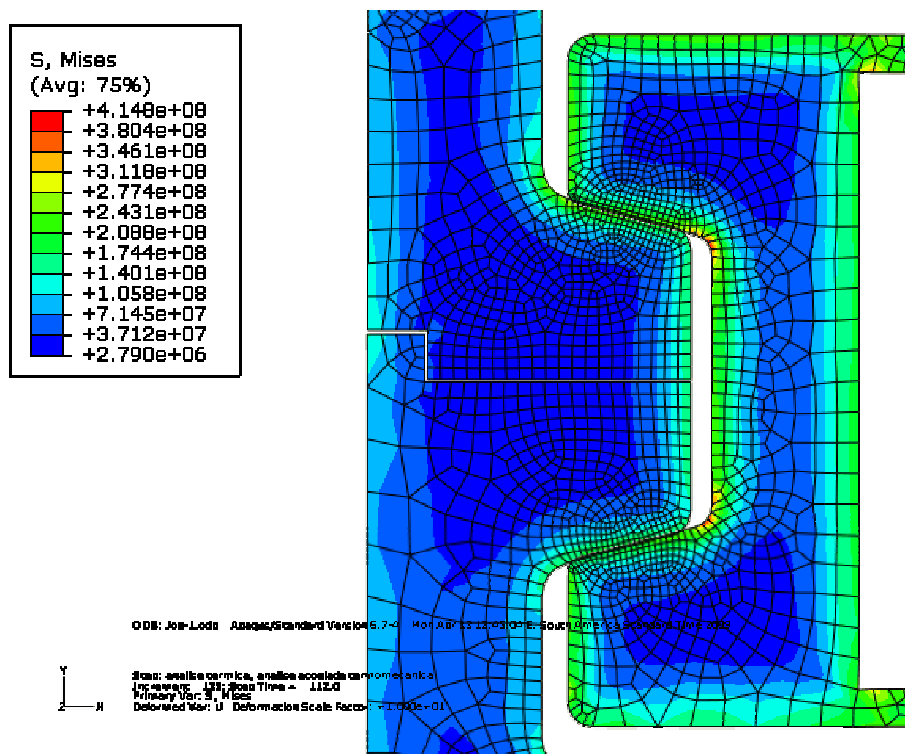
Figure 11. Von Mises stresses.

5. CONCLUSION

In this work the thermo-structural analysis of the VLS 4th stage separation system was performed. First, the aerodynamic heating was calculated, in order to determine the external boundary conditions of the domain. Then, using the FEM based ABAQUS software package, the temperature and thermal stresses distributions were calculated for the whole domain. It was observed that the maximum resulting stresses surpass the allowed limits in some specific points. As a consequence, the selected material depends on the use of an external thermal protection to be employed in the belt. It has to be emphasized that the results were obtained for the temperatures calculated during the first 112 seconds of flight.

6. REFERENCES

Anderson Jr., J.D., *Fundamentals of Aerodynamics*, McGraw-Hill, New York, 1990.

Anderson Jr., J.D., *Hypersonic and High Temperature Gas Dynamics*, AIAA Education Series, AIAA, New York, 1989.

Cline, P. B., 1969, "Entry Heat Transfer", in "Aerospace Applied Thermodynamics Manual – Part 4B", pp 517-598, SAE, NY.

Dassault Systèmes., "ABAQUS User's Manual", version 6.7, 2007.

Dhawan, S. and Narasimha, R., "Some Properties of Boundary Layer Flow During the Transition from Laminar to Turbulent Motion," *Journal of Fluid Mechanics*, Vol. 3, No. 4, 1958, pp. 418-436.

Machado, H.A. and Pessoa-Filho, J.B., "Aerodynamic Heating at Hypersonic Speeds," *Proceedings of 19th Brazilian Congress of Mechanical Engineering* [CD-ROM], Brasília, Brazil, 2007

Klausner,L and Machado,J.E, "Manual de Materiais Metálicos", CTA/IAE, São José dos Campos, Brazil, 1998 (in Portuguese).

Mazzoni, J.A., Pessoa Filho, J.B. e Machado, H.A., "Aerodynamic Heating on VSB-30 Sounding Rocket," *Proceedings of 18th Brazilian Congress of Mechanical Engineering* [CD-ROM], Ouro Preto, Brazil, 2005.

Miranda, I.F. and Mayall, M.C de M., "Convective Heat Flux in Micro-Satellites during the Atmospheric Reentry," Graduate Dissertation, Air Force Technical Institute - ITA, São José dos Campos, Brazil, 2001 (in Portuguese).

Rogan. J.E. and Hurwicz, H., "High-temperature Thermal Protection Systems," *Handbook of Heat Transfer*, edited by Rohsenow, W.M. and Hartnett J.P., McGraw-Hill, New York, 1973.

Surber, T. E., 1965, "Heat Transfer in the Vicinity of Surface Protuberances", J. Spacecraft, Vol. 2, no. 6, pp 978-980.

U.S. Standard Atmosphere, 1976.

Zoby, E.V., Moss, J.N. and Sutton, K., "Approximate Convective Heat Equations Hypersonic Flows," *Journal of Spacecraft and Rockets*, Vol. 18, No. 1, 1981, pp. 64-70.